

Unbalanced variation after assembly and double-speed influence coefficient method in the threshing drum

Zhiwu Yu^{1,2}, Yaoming Li^{1,2*}, Lizhang Xu^{1,2}, Xiaoxue Du^{1,2}, Kuizhou Ji^{1,2}

(1. Key Laboratory of Modern Agricultural Equipment and Technology, Ministry of Education, Jiangsu University, Zhenjiang 212013, Jiangsu, China;

2. School of Agricultural Engineering, Jiangsu University, Zhenjiang 212013, Jiangsu, China)

Abstract: Though the component of threshing drum is pre-balancing on the factory, the drum after assembly still has the problem of unbalanced vibration. In this study, the unbalance mechanism produced by assembly were introduced and the centroid propagation model in the series rotation system was established. The influence of the eccentricity and assembly phase on the assembly unbalance was studied. It is shown that there was a superposition effect between the initial centroid eccentricity caused by the machining error and the centroid eccentricity caused by assembly error, the unbalance amount under the in-phase assembly was larger than that of the anti-phase assembly. Moreover, the unbalance variation was experimentally investigated using in-field balancing detection on the test rig and combine harvester. The experiment results showed the excellent vibration reduction effect of in-field balancing, which showed a reduction of 83.0% and 85.8%. In order to increase the range of in-field balance detection and reduce the calculation error, the double-speed influence coefficient method was proposed. The proposed method adopted the way of first low-speed pre-balancing, and then high-speed precision balance, taking advantage of vibration information at two speeds and avoids nonlinear vibration conditions caused by high unbalanced vibration. Finally, the double-speed influence coefficient method was verified on the test rig. The vibration reduction effect of proposed method was better than the traditional method.

Keywords: unbalance variation, assembly, threshing drum, centroid propagation

DOI: [10.25165/j.ijabe.20231606.7651](https://doi.org/10.25165/j.ijabe.20231606.7651)

Citation: Yu Z W, Li Y M, Xu L Z, Du X X, Ji K Z. Unbalanced variation after assembly and double-speed influence coefficient method in the threshing drum. *Int J Agric & Biol Eng*, 2023; 16(6): 1–10.

1 Introduction

The unbalance of threshing drum will lead to bearing wear, reducing the use of components life and affect the reliability of the combine harvester^[1-3]. Through the online dynamic balance detection, the unbalance of the drum can be detected in the state of the whole machine, so as to compensate the error caused by assembly. Due to the characteristics of the double-side transmission of the combine harvester, the threshing drum after assembly forms a series rotation system^[4,5].

Although the individual components in a series rotation system is pre-balancing, there is still a certain amount of unbalance remaining limited by the accuracy of the balancing machine. Even if the residual unbalance of individual components is very small, all components after assembly can cause an unbalance of unacceptable level. Jolanta et al.^[6] presented the description of the process of the dynamic balancing of threshing drum in combine harvesters as well as the sources of unbalance. Tang et al.^[7] developed a dynamic

unbalance mode for grading chain drive double drums. The results showed that the unbalance of the drive load had an obvious effect on unbalanced amplitude of an active drum through the transfer characteristics of the chain drive. Li et al.^[8,9] established the dynamic response model of the multi-drum parallel system under different transmission modes and solved the vibration characteristics of the system. The above studies were mainly based on the dynamic response model to explain the influence of transmission on vibration characteristics. Actually, the vibration response of threshing drum is affected by many factors such as bearing, support and other vibration sources^[10]. The misalignment of inertial axis and rotation axis is the internal cause of unbalanced vibration. Transmission, bearing and other factors indirectly affect the output value of the vibration system by affecting the parameters of the vibration system. However, there was minor research on the analysis of unbalance vibration internal mechanism. This paper focus on the unbalance variation after the threshing drum is assembled to the combine harvester.

The unbalance of series rotation system is not only related to the residual unbalance of each component, but also the assembly error. Whitney et al.^[11,12] analyzed the error transfer in the assembly process, and realizes the description of the geometric tolerance by using the homogeneous matrix. Yang et al.^[13] used a probabilistic approach to analyze the influence of component variation on the eccentricity of the build and proposes a novel variation propagation control method in which individual components are re-orientated on a stage-by-stage basis to optimize the table-axis error for the final component in the assembly. Mao et al.^[14] developed a mathematical analysis method to predict the variation in an assembly process based on a state space equation. Sun et al.^[15] provided a novel

Received date: 2022-05-04 **Accepted date:** 2023-10-30

Biographies: **Zhiwu Yu**, PhD, Associate Researcher, research interest: intelligent agricultural equipment and technology, Email: yzwuj@163.com; **Lizhang Xu**, PhD, Associate Researcher, research interest: intelligent agricultural equipment and technology, Email: justxlz@ujs.edu.cn; **Xiaoxue Du**, PhD candidate, research interest: intelligent agricultural equipment and technology, Email: dx66610474@163.com; **Kuizhou Ji**, PhD candidate, Director, research interest: intelligent agricultural equipment and technology, Email: j kz_jkz@ujs@163.com.

***Corresponding author:** **Yaoming Li**, PhD, Professor, research interest: modern agricultural equipment, Jiangsu University, Zhenjiang, 212013, Jiangsu, China. Email: yml_i@126.com.

method to control the amount of unbalance propagation in precise cylindrical components assembly, which takes the machining error, the measurement error, and the assembly error into account. Liu et al.^[16] proposed a method to minimize stage-by-stage initial unbalance in the aero engine assembly of multistage rotors based on the connective assembly model. Above studies predict the unbalance of an assembly using a mathematical model and propose the optimization assembly methods to reduce the unbalance amount, experimental investigations are relatively limited. Therefore, the unbalance variation is studied using in-field balance detection and dynamic balancing machine.

Goodman^[17] proposed the influence coefficient method, which have become the most widely used method for rotor dynamic balancing technology. Several scholars have made improvements on the basis of the influence coefficient method for the particularity of application scenarios^[18,19]. Khulief et al.^[20] proposed a new method for field-balancing of high-speed flexible rotors combining both modal balancing and influence coefficient. Aiming to increase the robustness of the standard influence coefficient method, the rotor vibration responses measured over a long period are considered by means of a fuzzy transformation^[21]. Ranjan et al.^[22] utilized the influence coefficients obtained at high speed and unbalances identified at the low speed to effectively estimate the balance masses required for the high-speed flexible rotor balancing. The influence coefficient method is signal-based method that rely on the accuracy of measurement. However, the vibration environment is complex and measuring error is inevitable in field balancing detection. In-field balancing of the drum directly without pre-balancing may result in the catastrophic failure of the bearing housing and break the linear condition assumed by influence coefficient. So, there is a need to increase the detection range of in-field balance and reduce calculation errors.

The structure of this paper is as follows: Section 2 describes the model of centroid propagation in the series rotation system, and corresponding simulation results. Section 3 describes the experiment on the test rig and combine harvester, and studies the influence of the series component unbalance on the assembly as well as the unbalance variation after assembly. In section 4, the double-speed influence coefficient method is proposed and verified by experiments. Finally, the main conclusions are summarized in Section 5.

2 Model of centroid propagation in the series rotation system

2.1 Unbalance mechanism of series rotation system

According to the distribution of the unbalanced mass on the rotation shaft, the state of the rotor can be divided into static and moment unbalance, and dynamic unbalance is the combination of this two. The unbalanced mass u of the rotor causes the inertial axis is parallel offset to the rotation axis, therefore the centroid C does not coincide with the rotation axis (Figure 1). The unbalanced masses u_1 and u_2 are equal in amount and opposite in direction. The moment unbalance causes inertia axis to create an angle θ with respect to rotation axis, while the overall centroid C is located on rotation axis.

The rotor concentricity problem caused by assembly can also be described by the combination of the parallel offset and tilt of the inertial axis (Figure 2). These two conditions have different effect on the unbalance state. In the case of inertial axis parallel offset, the unbalance can be replaced by the effect produced by the unbalanced

mass u and the amount of unbalance is U_e . In the case of inertial axis tilt, the unbalance can be replaced by the effect of the unbalanced masses u_1 and u_2 , the amount of the unbalance is U_m .

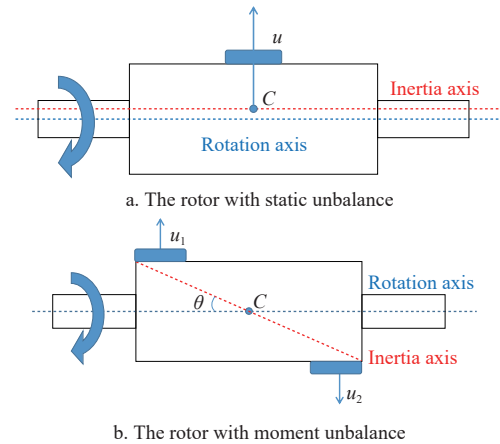


Figure 1 Unbalance classification

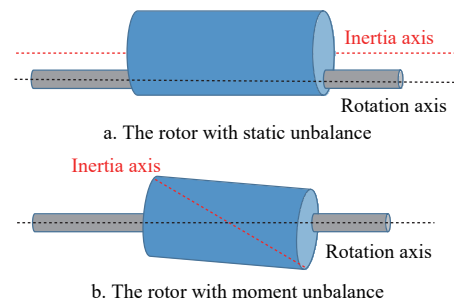


Figure 2 Unbalance produced by assembly

The equivalent unbalance to the inertial axis parallel offset can be calculated by the following equation:

$$U_e = m \times e \tag{1}$$

where, m is the rotor mass, g ; e is the distance between the inertial axis and the rotation axis, mm.

The equivalent unbalance to the inertial axis tilt (U_q) can be calculated by the following equation:

$$U_q = \theta(I_x - I_z) = u_1 r a \tag{2}$$

where, θ is the angle between the inertial axis and the rotation axis, °C; I_x is the X -axis inertia product, mm⁴; I_y is the Y -axis inertia product, mm⁴; u_1 is the unbalanced mass, g ; r is the distance from the unbalanced mass to the rotation axis, mm; a is the distance between two unbalanced mass, mm.

2.2 Mathematical model of centroid propagation in series rotation system

As the combine harvester has many rotation working components, the threshing drum has a bilateral transmission characteristic. After the threshing drum is assembled to the combine harvester, it forms a series rotation system (Figure 3). The threshing drum and transmission components are pre-balancing before

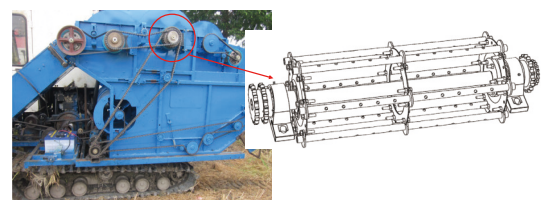


Figure 3 Series connection characteristic of the threshing drum

assembly. However, there is still a certain amount of unbalanced mass left limited by the machine error.

The influence of the residual unbalance on the series rotation system is mainly divided into two aspects. On the one hand, the residual unbalance directly affects the initial unbalance amount of the series rotation system; on the other hand, the eccentricity of the series rotation system is not only related to the residual unbalance but also related to the deviation of its positioning reference. Due to the unbalanced mass of the rotation component, the centroid is not on the center of rotation axis. After assembly errors, the centroid is further skewed, resulting in the further change of unbalance amount.

The assembly precision of the series rotation system is a crucial factor affecting the whole unbalance. It is necessary to ensure that the rotation center of each component is consistent with the rotation axis of shaft during the assembly process. In fact, due to component manufacturing tolerances and assembly process deviations, the center of each component is often deviated with the rotation axis. The eccentricity error and deflection error generated by each stage of rotation components are transmitted and accumulated, which lead to the change of the whole unbalance.

2.2.1 Model of centroid propagation under two components assembly

The concentricity of rotation component and threshing drum mainly depend on the machining accuracy. Due to the existence of machining errors, the radial fitting surface of the component is not an ideal surface. The axle hole fitting is used in the assembly. The machining error of the fitting surface is expressed as the deviation of the center position of the two components. The propagation process can be characterized by translation coordinate transformation. The schematic diagram of the fitting surface error is shown in Figure 4.

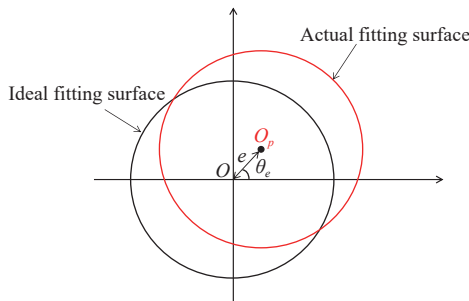


Figure 4 Schematic diagram of the fitting surface error

The error transfer matrix of the fitting surface is,

$$T^o = \begin{bmatrix} 1 & e \cos \theta_e \\ & 1 & e \sin \theta_e \\ & & 1 & z + dz \\ & & & 1 \end{bmatrix} \quad (3)$$

where, z is the ideal axial position of the fitting surface; dz is the axial machining error of the rotor.

The reason for the unbalance of assembly is that inertial axis and rotation axis do not coincide, and the unbalance is related to the position of centroid. In the series rotation system, the position of each component centroid needs to be accurately expressed, therefore this paper establishes the local coordinate system of each component and the global coordinate system of the assembly to express the change process of the centroid.

A global coordinate system is established with the center point of the first stage component, the center point of each component fitting surface is selected as the origin to establish a local coordinate

system. The model of centroid propagation under two components assembly is shown in Figure 5.

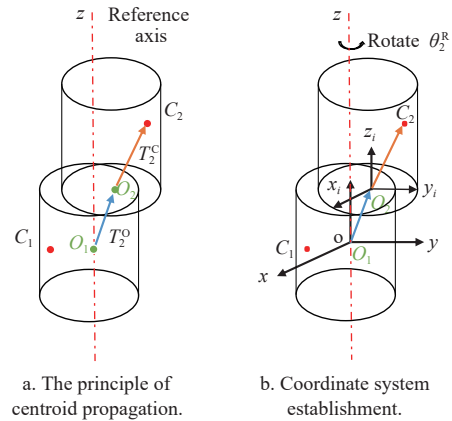


Figure 5 Model of centroid propagation under two components assembly

The coordinate position of centroid is related to the assembly phase of component. The assembly phase changes the centroid coordinate in the global coordinate system, but cannot change the centroid coordinate in the local coordinate system, which is equivalent to changing the local coordinate system position in the global coordinate system. The relationship between local and global coordinate system is affected by the machining error of fitting surface and assembly phase. The change of assembly phase can be described by the transformation of homogeneous coordinate. The centroid description in the global coordinate system can be obtained using coordinate transformation with the centroid position matrix and the fitting surface error transfer matrix in the local coordinate system.

The centroid position of the i th stage component in global coordinate system is described by the centroid transfer matrix T_{O-i}^C , and the centroid orientation in the local coordinate system is described by the centroid eccentricity matrix T_i^C .

$$T_{O-i}^C = T_i^o T_i^R T_i^C \quad (4)$$

where, T_i^o is the error transfer matrix of fitting surface; T_i^R is the assembly phase matrix, their mathematical expressions are,

$$T_i^o = \begin{bmatrix} dR_i^o & dP_i^o \\ 0^T & 1 \end{bmatrix} \quad (5)$$

where, dR_i^o is the 3×3 orientation matrix of fitting surface center, dP_i^o is the 3×1 position vector of fitting surface center. Since the first-stage component is the assembly reference of the series rotation system, dR_1^o and dP_1^o are the identity matrix and zero vector respectively.

The rotation transformation matrix dR_i^R is related to the angle θ_i^R rotated around the reference axis, and its mathematical expression is,

$$dR_i^R = \begin{bmatrix} \cos \theta_i^R & -\sin \theta_i^R & 0 \\ \sin \theta_i^R & \cos \theta_i^R & 0 \\ 0 & 0 & 1 \end{bmatrix} \quad (6)$$

The mathematical expression of the centroid eccentricity matrix T_i^C is,

$$T_i^C = \begin{bmatrix} dR_i^C & dP_i^C \\ 0^T & 1 \end{bmatrix} \quad (7)$$

where, dR_i^C is the direction matrix of the i th component centroid,

which is related to the direction of centroid. dP_i^c is the position vector of the centroid of the i th component, which is related to the local coordinate of centroid.

The local coordinate of the centroid of the i th component is known in the actual assembly, and the local coordinate of the centroid is,

$$dP_i^c = \begin{bmatrix} x_i^c \\ y_i^c \\ z_i^c \end{bmatrix} \quad (8)$$

The global coordinate of the centroid of the second stage component is,

$$T_{o-2}^c = T_2^o T_2^R T_2^c = \begin{bmatrix} dR_2^o & dP_2^o \\ 0^T & 1 \end{bmatrix} \begin{bmatrix} dR_2^R & 0 \\ 0^T & 1 \end{bmatrix} \begin{bmatrix} dR_2^c & dP_2^c \\ 0^T & 1 \end{bmatrix} = \begin{bmatrix} dR_2^o dR_2^R dR_2^c & dR_2^o dR_2^R dP_2^c + dP_2^o \\ 0 & 1 \end{bmatrix} \quad (9)$$

The position vector dP_{o-2}^c of the second stage component centroid in the global coordinate system is,

$$dP_{o-2}^c = dR_2^o dR_2^R dP_2^c + dP_2^o \quad (10)$$

$$dP_{o-2}^c = \begin{bmatrix} x_{o-2}^c \\ y_{o-2}^c \\ z_{o-2}^c \end{bmatrix} = \begin{bmatrix} x_2^c \cos \theta_2^R - y_2^c \sin \theta_2^R \\ x_2^c \cos \theta_2^R + y_2^c \sin \theta_2^R \\ z_2^c + z_1 + dz_1 \end{bmatrix} \quad (11)$$

According to the global coordinate of the second-stage component centroid and the global coordinate of the first-stage component centroid, the centroid coordinate of the entire assembly can be obtained, and the position vector dP^c of the assembly centroid:

$$dP^c = \frac{m_1}{m_1 + m_2} dP_{o-1}^c + \frac{m_2}{m_1 + m_2} dP_{o-2}^c \quad (12)$$

where, m_1 is the mass of the first stage component, g ; m_2 is the mass of the second stage component, g .

It can be known from the Equation (9) that the coordinate of assembly centroid in the global coordinate system is,

$$X^c = \frac{m_1}{m_1 + m_2} x_1^c + \frac{m_2}{m_1 + m_2} x_2^c \quad (13)$$

$$Y^c = \frac{m_1}{m_1 + m_2} y_1^c + \frac{m_2}{m_1 + m_2} y_2^c \quad (14)$$

The overall unbalance is the product of centroid eccentricity and component mass, then U_2 is,

$$U_2 = \sum_{i=1}^2 m_i \sqrt{(X^c)^2 + (Y^c)^2} \quad (15)$$

2.2.2 Model of centroid propagation under three components assembly

The model of centroid propagation under three components assembly is shown as Figure 6, the assembled centroid transfer matrix T_{o-3}^c is,

$$T_{o-3}^c = T_2^o T_2^R T_3^o T_3^R T_3^c \quad (16)$$

$$T_{o-3}^c = T_2^o T_2^R T_3^o T_3^R T_3^c = \begin{bmatrix} dR_2^o & dP_2^o \\ 0^T & 1 \end{bmatrix} \begin{bmatrix} dR_2^R & 0 \\ 0^T & 1 \end{bmatrix} \begin{bmatrix} dR_3^o & dP_3^o \\ 0^T & 1 \end{bmatrix} \begin{bmatrix} dR_3^R & 0 \\ 0^T & 1 \end{bmatrix} \begin{bmatrix} dR_3^c & dP_3^c \\ 0^T & 1 \end{bmatrix} = \begin{bmatrix} dR_2^o dR_2^R dR_3^o dR_3^R dR_3^c & dR_2^o dR_2^R dR_3^o dR_3^R dP_3^c + dR_2^o dR_2^R dP_3^o + dP_2^o \\ 0 & 0 \end{bmatrix} \quad (17)$$

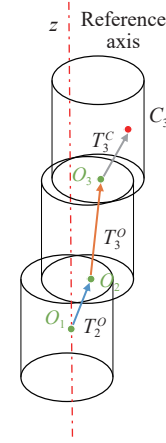


Figure 6 Model of centroid propagation under three components assembly

The position vector dP_{o-3}^c of the second stage component centroid in the global coordinate system is,

$$dP_{o-3}^c = dR_2^o dR_2^R dR_3^o dR_3^R dP_3^c + dR_2^o dR_2^R dP_3^o + dP_2^o \quad (18)$$

$$dP_{o-3}^c = \begin{bmatrix} x_{o-3}^c \\ y_{o-3}^c \\ z_{o-3}^c \end{bmatrix} = \begin{bmatrix} x_3^c \cos(\theta_2^R + \theta_3^R) - y_3^c \sin(\theta_2^R + \theta_3^R) \\ x_3^c \cos(\theta_2^R + \theta_3^R) + y_3^c \sin(\theta_2^R + \theta_3^R) \\ z_3^c + z_2 + dz_2 + z_1 + dz_1 \end{bmatrix} \quad (19)$$

The position vector dP^c of the assembly centroid can be expressed as:

$$dP^c = \frac{m_1}{m_1 + m_2 + m_3} dP_{o-1}^c + \frac{m_2}{m_1 + m_2 + m_3} dP_{o-2}^c + \frac{m_3}{m_1 + m_2 + m_3} dP_{o-3}^c \quad (20)$$

where, m_1 is the mass of the first stage component, m_2 is the mass of the second stage component, and m_3 is the mass of the third stage component.

It can be known from the Equations (10) and (18) that the coordinate of assembly centroid in the global coordinate system is:

$$X^c = \frac{m_1}{m_1 + m_2 + m_3} x_1^c + \frac{m_2}{m_1 + m_2 + m_3} x_2^c + \frac{m_3}{m_1 + m_2 + m_3} x_3^c \quad (21)$$

$$Y^c = \frac{m_1}{m_1 + m_2 + m_3} y_1^c + \frac{m_2}{m_1 + m_2 + m_3} y_2^c + \frac{m_3}{m_1 + m_2 + m_3} y_3^c \quad (22)$$

The overall unbalance is the product of centroid eccentricity and component mass, then U_3 is

$$U_3 = \sum_{i=1}^3 m_i \sqrt{(X^c)^2 + (Y^c)^2} \quad (23)$$

2.3 Simulation results of the centroid propagation model

According to the model of centroid propagation under three component assembly, the height of the first and third stage components is 50 mm, the radius is 50 mm, and the mass is 5 kg. The height of the second stage rotor is 600 mm, the radius is 150 mm, and the mass is 30 kg. The eccentricity of fitting surface is 0.10 mm, 0.12 mm, 0.14 mm, 0.16 mm, 0.18 mm, 0.20 mm, and the two fitting surfaces eccentricity is equal. The axial machining error of the fitting surface is 0. It is assumed that each stage of the component has a residual unbalanced mass of 20 g on the outer surface and has the same initial position due to the accuracy error of the pre-balancing machine.

With the change of the assembly phase between the components, the unbalance of the assembly decreases first and then increases, as shown in Figure 7. When the assembly phase is 180°,

the unbalance of the assembly has a minimum amount and is symmetrically distributed around 180°. The main reason is that the unbalance between the components has the same direction under the initial condition. With the increase of the phase angle, the unbalance conforms to the vector superposition theorem. Taking the data that the eccentricity of fitting surface is 0.1 mm as an example, the minimum unbalance amount is 1000 g·mm when the model is anti-phase assembly, and the maximum unbalance amount is 6500 g·mm when the model is in-phase assembly. The unbalance amount of the assembly increases by 5.5 times. It is shown that the assembly phase between the components is crucial to the overall unbalance.

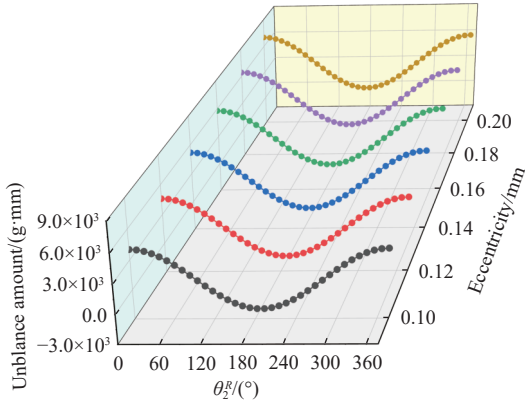


Figure 7 Simulation under two components assembly

The amount of eccentricity also affects the assembly unbalance. As the amount of eccentricity increases, the amount of unbalance also increases gradually. Figure 7 shows that there is a superposition effect between the initial centroid eccentricity caused by the machining error and the centroid eccentricity caused by assembly error. It is proved that the unbalance of the series rotation system after assembly is the vector superposition of the unbalance of each rotation component.

Simulation under three components assembly is shown in Figure 8. With the change of the assembly phase of the second and third stage component, the unbalance of the assembly varies between 500 g·mm and 8500 g·mm. When the assemble phase of the second and third stage rotors is 180°, the unbalance of assembly has a minimum amount, which is 500 g·mm. When the installation phase of the second and third stage rotors is 0°, the unbalance of assembly has a maximum amount, which is 8500 g·mm.

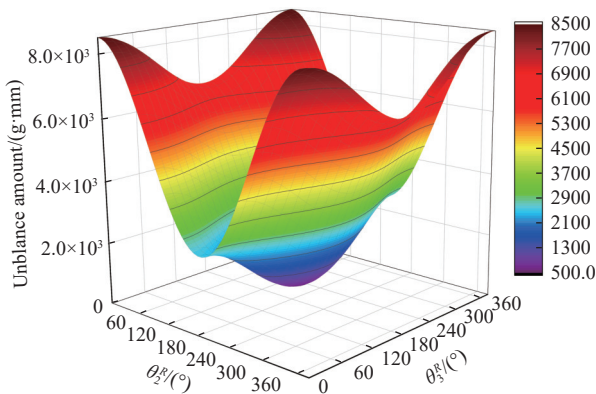


Figure 8 Simulation under three components assembly

3 Experiment on the test rig and combine harvester

3.1 Influence of the series component unbalance on the assembly

The S956Y-1 dynamic balance detector, vibration velocity

sensor, and photoelectric speed sensor are used for testing. The parameters of instrument are listed in Table 1.

Table 1 Parameters of instrument

Instrument name	Model	Performance target	Parameters	Picture
Dynamic balance detector	S956Y-1	Frequency Range/Hz	10-5000	
		Frequency response error/%	±5	
		Maximum range/mm·s ⁻¹	100	
		Highest resolution/mm·s ⁻¹	0.1	
Acceleration sensor	L14A	Sensitivity/pc·m ⁻¹ ·s ⁻²	3.5-5.2	
		Frequency Range/Hz	2-3000	
		Maximum acceleration/m·s ⁻²	2000	
Photoelectric speed sensor	SGD-1-5V	Measuring range/r·min ⁻¹	1-60 000	
		Operating Voltage/V DC	5	
		Output signal type	TTL Pulse signal	

The threshing drum structure of the test rig is shown in Figure 9. During the experiment, the drum speed is increased from 300 r/min to 500 r/min, and the speed is increased by 50 r/min each time. After the speed is relatively stable, the unbalanced vibration signal is collected. In order to study the influence of component unbalance on the series rotation system, it is simulated by artificially adding the unbalanced mass and 4 kinds of unbalanced mass (50 g, 100 g, 150 g, 200 g) is added to the radius of 135 mm of the balance disk, fix them with bolts and load them in the same phase. The assembly position of sensor and unbalanced mass is shown in Figure 10.

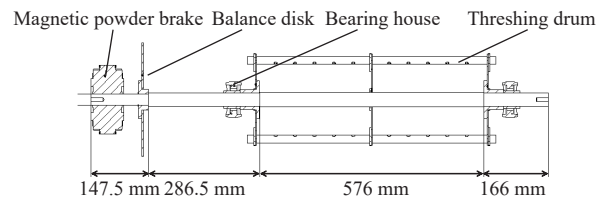


Figure 9 Schematic diagram of the structure of the threshing drum

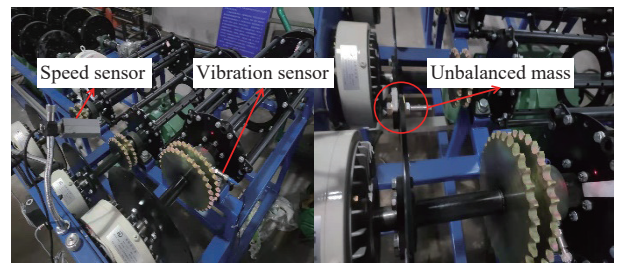


Figure 10 Assembly position of sensor and unbalanced mass

In order to study the influence of the series component unbalance on the rotation system, 100 g unbalanced mass is added inside and outside the drum respectively, and the vibration responses of the bearing housing under four working conditions are collected. The schematic diagrams of the four working conditions are shown in Figure 11.

It can be seen from Table 2 that the amplitude of the fundamental frequency increase monotonically with the increase of

the rotation speed, but the vibration amplitude does not increase proportionally as the unbalanced mass increases. Compared with the influence of the unbalanced mass on the vibration response, the rotation speed has a greater impact on the unbalanced vibration response. Under the condition of rotation speed of 300 r/min, the amplitude is 0.092 mm/s when the unbalanced mass is 0 g, the amplitude is 0.622 mm/s when the unbalanced mass is 50 g, and the amplitude is 0.669 r/min when the unbalanced mass is 200 g. Compared with the change of the amplitude under the unbalanced mass of 0-50 g, the change of the amplitude under the unbalanced mass of 50-200 g is not obvious. So the effects of optimization assembly method proposed by Sun et al.^[15] and Liu et al.^[16] are really limited. These methods can reduce the amount of unbalance, but cannot significantly reduce the unbalance vibration. The existence of the component unbalanced mass has a greater impact on the vibration state of the rotation system. The influence of the series component on the vibration of the threshing drum depends not only on the amount of the unbalance, but also on the distribution form of the unbalance. The change of the series rotation system vibration response is studied under different working conditions.

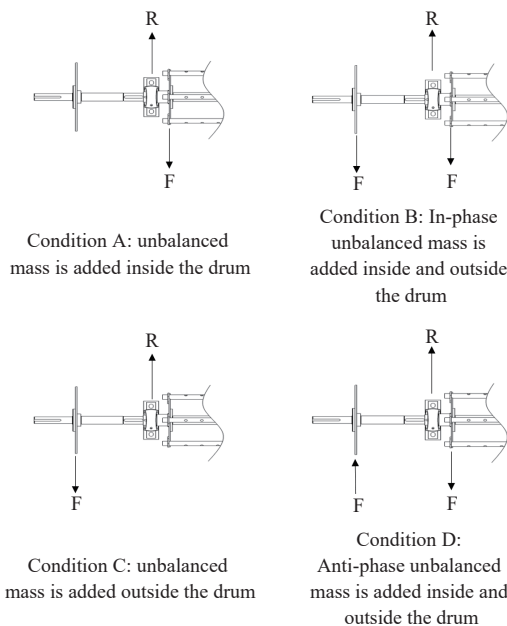


Figure 11 Schematic diagram of four working conditions

Table 2 Amplitude of unbalance vibration

Speed/ r·min ⁻¹	Unbalanced mass				
	0	50 g	100 g	150 g	200 g
300	0.092	0.622	0.544	0.690	0.669
350	0.131	0.867	0.846	0.932	0.940
400	0.133	1.073	0.907	1.210	1.362
450	0.114	1.151	1.001	1.534	1.867
500	0.152	1.295	1.303	2.099	2.688

From the comparison of the unbalance vibration under different working conditions in Table 3, it can be seen that the amplitude of the A working condition is greater than that of the C working condition at the five rotational speeds, indicating that the vibration response caused by the unbalance inside the drum is greater than the outside. The addition of anti-phase unbalanced mass on the series rotation system will cause the moment unbalance, and the vibration response caused by the moment unbalance is greater than the vibration response under the A and C conditions. Although the

unbalance vector is 0 under the condition D, the unbalance moment is very large. The vibration amplitude under working condition B is greater than that under working condition D, which reflects that the unbalance mass under the in-phase assembly is larger than that of the anti-phase assembly, which is consistent with the simulation results.

Table 3 Amplitude under four working conditions

Speed/r·min ⁻¹	A	B	C	D
300	0.592	0.681	0.544	0.636
350	0.897	1.035	0.846	0.789
400	1.139	1.322	0.907	0.999
450	1.314	1.858	1.001	1.156
500	1.582	2.542	1.303	1.211

3.2 Unbalance variation after assembly

Existing research rarely uses dynamic balance detection equipment to reflect the change of unbalanced mass after rotor is assembled to whole machine. In this study, the unbalanced mass of a single drum is measured by dynamic balancing machine, and the unbalanced mass after assembly is measured by an in-field balancing detection, and the change of unbalanced mass is revealed through the comparison before and after assembly. To reduce the error of the detection system and improve the signal noise ratio of the dynamic balance detection, a certain unbalanced mass is reserved on the drum. The unbalanced mass can be obtained by the dynamic balancing machine (Figure 12).

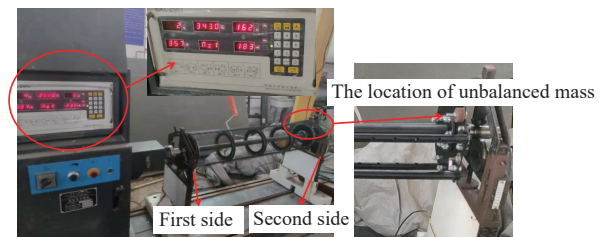


Figure 12 Threshing drum on the dynamic balancing machine

The drum is placed on the hard bearing dynamic balancing machine (Model HW-500 Zhong Lian Co., Ltd, China), and the rotational speed is 343 r/min. The unbalanced mass of the drum on the second side measured by the dynamic balancing machine is 162 g and the unbalanced mass on the first side is 2 g. The location is shown in Figure 13.

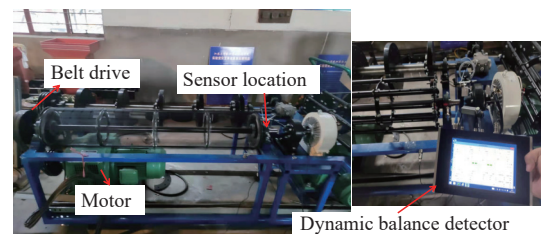


Figure 13 Threshing drum on the test rig

The threshing drum is installed on the test rig and connected to motor through belt drive (Figure 13). In-field balance detection is done with S956Y-1 dynamic balance detector. In order to avoid the interference of the transmission vibration, the horizontal direction of bearing housing near the second side is taken as the installation point of the vibration accelerate sensor, and the influence coefficient method is used to convert vibration response into unbalanced mass. In this study, the mechanism of the unbalanced

force is revealed through the position of centroid, and the effect of the unbalanced moment is not involved. In the experiment, the in-field balance method is also used to make the vector sum of the unbalanced force zero. As the working speed of the drum is much smaller than the critical speed, the threshing drum can be regarded as a rigid rotor, and the influence of the speed on the unbalanced mass measurement can be ignored.

162 g correction mass is added to the shield according to the result on the dynamic balancing machine, the unbalance vibration at the bearing housing is 0.112 mm/s. Continue the in-field balance operation, the unbalance vibration is reduced to 0.019 mm/s when 153.89 g mass is added.

The positions of the two detection results on the shield are shown in Figure 14. The red is the detection result by the dynamic balancing machine, and the blue is the detection result by the in-field balancing detector. By subtracting the two vectors, the difference between the two can be calculated as 42 g. The vibration is reduced by 83% after in-field balancing.

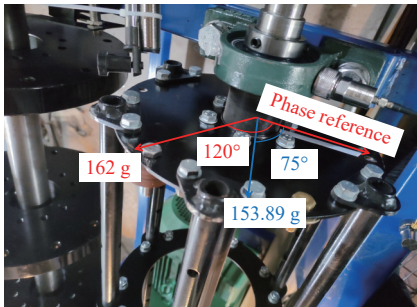


Figure 14 Position of the two measurements on the shield

Furthermore, experiment is carried out on the threshing drum of combine harvester (Model GN120 (4LZ-12) Foton Lovol International Heavy Industry Co., Ltd, China). The mass of the threshing drum is 300 kg, the correction radius is 300mm, and the balance speed is 620 r/min. The unbalanced mass of the drum is measured by the dynamic balancing machine (Model DH1000W Shanghai Move Also Static Testing Machine Co., Ltd, China) and the in-field balancing detector respectively (Figure 15). The experiment operation steps are the same as the previous.



a. Dynamic balancing machine



b. In-field balancing detection

Figure 15 Two measurements on the threshing drum

300 g corrected mass is added to the surface of the drum according to the result on the dynamic balancing machine, the unbalance vibration at the bearing housing is 8.32 mm/s. The vibration amplitude is 1.18 mm/s when the corrected mass is 500 g. The vibration is reduced by 85.8% after in-field balancing. The vector difference of the corrected mass is 61 g. The location of the two measurements on the threshing drum is shown in Figure 16.

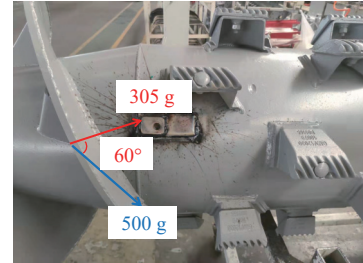


Figure 16 Position of the two measurements on the threshing drum

The unbalanced mass has changed when the threshing drum is assembled to the combine harvester. After the in-field balance correction, the unbalance vibration amplitude will be further reduced, which reflects the advantages of the in-field balance. There are many reasons for this unbalanced mass change, which can be mainly explained from the following aspects:

1) The principle of dynamic balancing machine and in-field balancing are different. The hard support dynamic balancing machine adopts the form of rollers to support the rotor to rotate, and the in-field balancing detection is carried out on its own bearing housing, so the supporting stiffness is inconsistent. Besides the dynamic balancing machine uses force sensors and statics to analyze the unbalanced mass, while the online dynamic balancing measurement uses a magnetic vibration acceleration sensor. The vibration sensor is attached to the bearing housing and use signal-based method to analyze the unbalanced mass.

2) The vibration environment is complex during in-field balancing. Under the same measurement conditions, the vibration response obtained by measuring a rotor with a certain amount of unbalance is not a fixed value but a data set with a certain dispersion, random errors are inevitable^[21]. Moreover, the influence coefficient is obtained by adding the trail weight in in-field balance. The quality of the trail weight determines the accuracy of the calibration model, which is crucial for the correction of the in-field balancing. The influence coefficient method is a signal-based method. The unbalanced response per unit mass is obtained by adding trail weight, and then the unbalanced mass and phase are calculated by dividing the initial vibration response by the influence coefficient. The influence coefficient method aims to reduce the vibration response at the housing rather than actually reduce the unbalance of the threshing drum, the influence coefficient method will convert all fundamental frequency vibration responses into the unbalanced masses, which is also the main reason for the inconsistency between the in-field balancing data and the machine data.

3) The assembly error is inevitable during the assembly of the drum to the machine. The assembly error can be divided into: bearing assembly deviation, bearing concentricity deviation, transmission component and rotor connection deviation, machine and foundation installation deviation. Bearing assembly deviation mainly refers to the gap between the rotor journal and the bearing, the fit deviation between the bearing and the bearing housing, and

the installation error between the bearing housing and frame^[23]. Bearing concentricity deviation mainly refers to the concentricity deviation between two or more bearings^[24]. The connection deviation between the transmission component and the rotor refers to the clearance and concentricity deviation between the drive wheel and the rotor shaft. The deviation between the machine and the foundation installation mainly refers to the deviation of the connection stiffness between the machine and the foundation, and the deviation of the machine installation levelness. These assembly errors will lead to the inconsistency between the inertial axis and the rotational axis, so the unbalanced mass will change to some extent^[25].

In-field dynamic balancing can solve the vibration problem after the drum is assembled to the whole machine, and compensate the error of assembly to a certain extent, which can further reduce the vibration response at the bearing housing. In-field balancing has a greater advantage over dynamic balancing machine.

4 Double-speed influence coefficient method

Since the threshing drum after manufacturing has a large amount of unbalance, the dynamic balancing machine is widely used in industry. It can be seen that in-field balancing has a greater advantage over pre-balancing, therefore the in-field balance method is used to balance the threshing drum to replace pre-balancing technique. However, if the unbalanced vibration is too large, other excitation sources of the combine harvester will be induced, resulting in the change of the vibration environment and the breaking of the linear working condition of the vibration. In order to increase the range of in-field balance detection and reduce the detection error, the double-speed influence coefficient method has been proposed. The proposed method adopts the way of first low-speed pre-balancing, and then high-speed precise balance. The vibration is reduced to a reasonable range through low-speed pre-balancing, and then the counterweight is calculated through high-speed precision balance.

Taking the single-side balance as an example, the main idea of the double-speed influence coefficient method is introduced.

$$\vec{V} = \vec{X} + \vec{Y} \quad (24)$$

where, \vec{X} is the actual unbalanced vibration response; \vec{Y} is the measurement error of the detection system; and the fundamental frequency vibration response obtained by the detection system is \vec{V} .

$$\vec{V}_{01} = \vec{X}_1 + \vec{Y}_1 \quad (25)$$

$$\vec{V}_{M1} = \vec{X}_{M1} + \vec{Y}_1 \quad (26)$$

where, \vec{M}_1 is the initial trail weight vector; \vec{V}_M is the vibration response after the trail weight; \vec{V}_0 is the initial vibration response.

First the low-speed initial balance is performed on the threshing drum to obtain the influence coefficient $\vec{\alpha}_1$:

$$\vec{\alpha}_1 = \frac{\vec{V}_{M1} - \vec{V}_{01}}{\vec{M}_1} = \frac{\vec{X}_{M1} - \vec{X}_1}{\vec{M}_1} \quad (27)$$

Then the high-speed dynamic balance is performed on the threshing drum. The trial weight vector \vec{M}_2 is added to get the influence coefficient $\vec{\alpha}_2$:

$$\vec{V}_{02} = \vec{X}_2 + \vec{Y}_2 \quad (28)$$

$$\vec{V}_{M2} = \vec{X}_{M2} + \vec{Y}_2 \quad (29)$$

$$\vec{\alpha}_2 = \frac{\vec{V}_{M2} - \vec{V}_{02}}{\vec{M}_2} = \frac{\vec{X}_{M2} - \vec{X}_2}{\vec{M}_2} \quad (30)$$

Let the initial unbalance vector be \vec{M}_0 , then

$$\vec{X}_1 = \vec{\alpha}_1 \times \vec{M}_0 \quad (31)$$

$$\vec{X}_2 = \vec{\alpha}_2 \times \vec{M}_0 \quad (32)$$

Due to the existence of measurement error, \vec{X}_1 is difficult to measure directly, so it is usually replaced by \vec{V}_{01} , which leads to the calculation error of the detection system. The measurement error can be offset by subtracting the influence coefficients.

$$(\vec{\alpha}_2 - \vec{\alpha}_1) \times \vec{M}_0 = \vec{X}_2 - \vec{X}_1 \quad (33)$$

$$\vec{X}_2 - \vec{X}_1 = (\vec{V}_{02} - \vec{Y}_2) - (\vec{V}_{01} - \vec{Y}_1) = \vec{V}_{02} - \vec{V}_{01} - \Delta\vec{Y}_{12} \quad (34)$$

In the case of the vibration structure and the sensor position unchanged, the random vibration has a constant value, the change of the measurement error with the rotation speed is very small and can be ignored, so it can be obtained:

$$\Delta\vec{\alpha} = \frac{\vec{V}_{M2} - \vec{V}_{02}}{\vec{M}_2} - \frac{\vec{V}_{M1} - \vec{V}_{01}}{\vec{M}_1} \quad (35)$$

Through the double-speed influence coefficient method, the full use of the vibration information at the two speeds can make up for the lack of measurement accuracy.

In order to verify the balancing effect of the double-speed influence coefficient method, the S956Y-1 dynamic balance detector is used to measure the vibration response at the bearing housing. The double speed influence coefficient method is used to get the counterweight at the balance speed of 300 r/min and 600 r/min. The traditional influence coefficient method is used to get the counterweight at the balance speed of 600 r/min, as a comparative experiment. The trail weight and counterweight parameters under the two methods are listed in Table 4, and the added position of the mass is shown in Figure 17.

Table 4 Trail weight and counterweight parameters under the two methods

Method	Speed/r·min ⁻¹	TM	TMP	CWM	CWMP
Double-speed method	300	210	21	125	34
	600	72	163	96	54
Traditional method	600	334	169	278	56

Note: TM-Trial mass; TMP-Trial mass phase; CWM-counterweight mass CWMP-Counterweight mass phase.

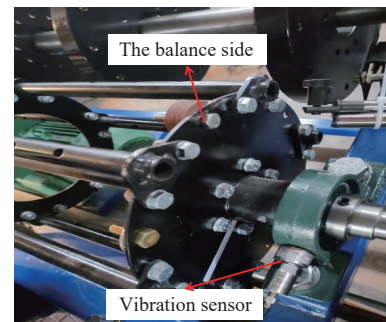


Figure 17 Added position of the mass

The counterweight is added to the drum and the vibration signal at the bearing housing is collected with a vibration acceleration sensor. The sampling frequency is 2000 and the low-pass filtering is

used to process the data.

It can be seen from Figure 18 that the vibration amplitude of the double-speed method is smaller than that of the traditional method at sub-synchronous, synchronous and super-synchronous. The amplitude reduction rate is greatest at synchronous, decreasing from 0.093 m/s^2 to 0.023 m/s^2 , which shows a reduction of 42.6%. The vibration reduction effect of the double-speed influence coefficient method is better than that of the traditional balancing method.

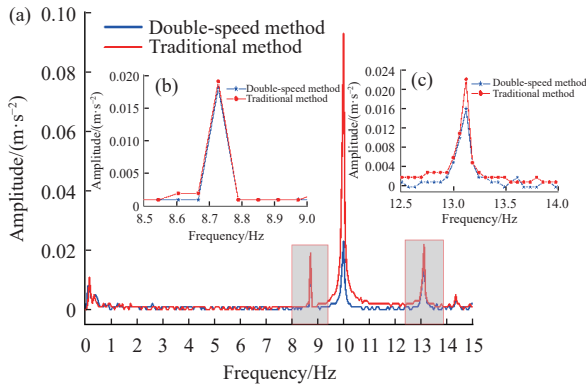


Figure 18 Vibration amplitudes of the two methods at different frequencies

In recent years, several methods based on influence coefficient have been developed but only few seem to be suitable for industrial applications. Ranjan et al.^[22] utilize the unbalances estimated at the low speeds to balance the rotor system periodically. The experiment is shown that the change in influence coefficients at low-speed does not affect the estimation as no mode shapes are formed. Zhou et al.^[26] proposed an online unbalance compensation algorithm with active magnetic bearings based on the least mean squares method and the influence coefficient method. The proposed algorithm is to suppress the unbalance vibration of the rotor and achieve the online unbalance compensation of the maglev rotor. Alves et al.^[10] propose a method that uses acceleration of bearing housing in influence coefficients avoiding problems related to oil film nonlinearities. In order to increasing the robustness of the influence method, a preprocessing stage is applied to access the uncertainties affecting the rotating machine. In this sense, measurement data sets evaluated under the fuzzy logic approach are used^[21]. Compared with these existing methods, the proposed method takes advantage of vibration information at two speeds and avoids nonlinear vibration conditions caused by high unbalanced vibration. Moreover, the effect of measurement error on unbalance estimation is reduced by influence coefficient subtraction.

5 Conclusions

In order to solve the unbalanced vibration after the threshing drum is assembled to the combine harvester, the centroid propagation model of the series rotation system was established. The simulation result is shown that there is a superposition effect between the initial centroid eccentricity caused by the machining error and the centroid eccentricity caused by assembly error. Moreover, the unbalance of the series rotation system after assembly is the vector superposition of the unbalance of each rotation component. Experiment on the test rig is shown that the unbalance mass under the in-phase assembly is larger than that of the anti-phase assembly, which is consistent with the simulation results. Then the change of unbalanced mass after assembly is

studied on the test rig and combine harvester. In-field balancing can solve the vibration problem after the drum is assembled to the whole machine, and compensate the error of assembly to a certain extent, which can further reduce the vibration response at the bearing housing. After in-field balancing, the vibrations are reduced by 83.0% and 85.8%, respectively. In order to increase the range of in-field balance detection and reduce the detection error, the double-speed influence coefficient method has been proposed. The vibration reduction effect of the double-speed influence coefficient method is better than the traditional balancing method.

Acknowledgements

The authors gratefully acknowledge the National Natural Science Foundation of China (Grant No. 51975257), National Key Research and Development Project (Grant No. 2017YFD0700200).

[References]

- [1] Yu Z W, Li Y M, Wang X Z, Tang Z, Lu J H. Effects of side load chains of a combine harvester on unbalanced dynamic vibrations of its threshing drum. *International Journal of Rotating Machinery*, 2021; 2021(8): 1–13.
- [2] Tang Z, Li Y, Li X Y. Structural damage modes for rice stalks undergoing threshing. *Biosystems Engineering*, 2019; 186(1): 323–336.
- [3] Gao Z P, Xu L Z, Li Y M, Wang Y D, Sun P P. Vibration measure and analysis of crawler-type rice and wheat combine harvester in field harvesting condition. *Transactions of the CSAE*, 2017; 33(20): 48–55.
- [4] Chen S R, Zhou Y P, Tang Z, Lu S N. Modal vibration response of rice combine harvester frame under multi-source excitation. *Biosystems Engineering*, 2020; 194: 177–195.
- [5] Pang J, Li Y M, Ji J T, Xu L Z. Vibration excitation identification and control of the cutter of a combine harvester using triaxial accelerometers and partial coherence sorting. *Biosystems Engineering*, 2019; 185: 25–34.
- [6] Krolczyk J B, Legutko S, Krolczyk G M. Dynamic balancing of the threshing drum in combine harvesters – the process, sources of imbalance and negative impact of mechanical vibrations. *Applied Mechanics and Materials*, 2014; 693: 424–429.
- [7] Tang Z, Li X Y, Liu X, Ren H, Zhang B. Dynamic balance method for grading the chain drive double threshing drum of a combine harvester. *Applied Sciences*, 2020; 10(3): 1026.
- [8] Li Y, Tang Z, Wang X Z, Zhang H, Li Y M. Bearing seat vibration modes undergoing unbalanced excitation of multirotating drums. *Shock and Vibration*, 2021; 2021: 1–20.
- [9] Li Y, Tang Z, Zhang B, Wang M L. Vibration transmission characteristics and detection method of bilateral chain drive of multicylinders. *Mathematical Problems in Engineering*, 2021; 2021: 1–22.
- [10] Alves D S, Machado T H, Cavalca K L, Bachschmid N. Characteristics of oil film nonlinearity in bearings and its effects in rotor balancing. *Journal of Sound and Vibration*, 2019; 459: 114854.
- [11] Whitney D E, Gilbert O L, Jastrzebski M. Representation of geometric variations using matrix transforms for statistical tolerance analysis in assemblies. *Research in Engineering Design*, 1994; 6: 191–210.
- [12] Whitney D E. *Mechanical assemblies*. Oxford: Oxford University Press, 2004; 542p.
- [13] Yang Z, McWilliam S, Popov A A, Hussain T. A probabilistic approach to variation propagation control for straight build in mechanical assembly. *International Journal of Advanced Manufacturing Technology*, 2013; 64: 1029–1047.
- [14] Mao J, Chen D J, Zhang, L Q. Mechanical assembly quality prediction method based on state space model. *The International Journal of Advanced Manufacturing Technology*, 2016; 86: 107–116.
- [15] Sun C Z, Hu M, Liu Y M, Zhang M W, Liu Z W, Chen D Y, et al. A method to control the amount of unbalance propagation in precise cylindrical components assembly. *Proceedings of the Institution of Mechanical Engineers Part B Journal of Engineering Manufacture*, 2019; 233(13): 2458–2468.
- [16] Liu Y M, Zhang M W, Sun C Z, Hu M, Chen D Y, Liu Z W, Tan J B. A method to minimize stage-by-stage initial unbalance in the aero engine assembly of multistage rotors. *Aerospace Science and Technology*, 2019; 85: 270–276.
- [17] Goodman T P. A least-squares method for computing balance corrections.

- [Journal of Manufacturing Science & Engineering](#), 1964; 86(3): 273–277.
- [18] Parkinson A G, Darlow M S, Smalley A J. A theoretical introduction to the development of a unified approach to flexible rotor balancing. [Journal of Sound & Vibration](#), 1980; 68(4): 489–506.
- [19] Hassan G A. New approach for computer-aided static and dynamic balancing of rigid rotors. [Journal of Sound & Vibration](#), 1995; 179(5): 749–761.
- [20] Khulief Y A, Mohiuddin M A, El-Gebeily M. A new method for field-balancing of high-speed flexible rotors without trial weights. [International Journal of Rotating Machinery](#), 2014; 2014: 1–11.
- [21] Carvalho V N, Rende B N, Silva A D G, Cavalini A A, Steffen V. Robust balancing approach for rotating machines based on fuzzy logic. [Journal of Vibration & Acoustics](#), 2018; 140(5): 051018.
- [22] Ranjan G, Tiwari R. On-site high-speed balancing of flexible rotor-bearing system using virtual trial unbalances at slow run. [International Journal of Mechanical Sciences](#), 2020; 183: 105786.
- [23] Cao H R, Shi F, Li Y M, Li B J, Chen X F. Vibration and stability analysis of rotor-bearing-pedestal system due to clearance fit. [Mechanical Systems and Signal Processing](#), 2019; 133: 106275.
- [24] Wang N F, Jiang D X. Vibration response characteristics of a dual-rotor with unbalance-misalignment coupling faults: theoretical analysis and experimental study. [Mechanism and Machine Theory](#), 2018; 2018: 207–219.
- [25] Li Z G, Jiang J, Tian Z. Non-linear vibration of an angular-misaligned rotor system with uncertain parameters. [Journal of Vibration & Control](#), 2016; 22: 129–144.
- [26] Zhou J, Wu H C, Wang W Y, Yang K Z, Hu Y F, Guo X H, et al. Online unbalance compensation of a maglev rotor with two active magnetic bearings based on the LMS algorithm and the influence coefficient method. [Mechanical Systems and Signal Processing](#), 2022; 166: 108460.